

The neutron star inner crust: an empirical essay

Luiz L. Lopes*

Centro Federal de Educação Tecnológica de Minas Gerais Campus VIII, CEP 37.022-560, Varginha, MG, Brasil

(Dated: August 18, 2021)

In this work I study how the small contribution of the inner crust to the total equation of state (EoS) of a neutron star affects its mass-radius relation, focusing on the canonical mass of $1.4M_{\odot}$. I build a polytropic empirical EoS of the kind: $p = K\epsilon^{\gamma} + b$, in the range of $0.003 \text{ fm}^{-3} < n < 0.08 \text{ fm}^{-3}$ and also calculate the speed of sound in this region. We see that different behaviours of the speed of sound can affect the radius of the canonical star by more than 1.1 km. This result can help us understand extreme results as GW170817, where some studies indicate that the radius of the canonical star cannot exceed 11.9 km.

I. INTRODUCTION

The physics of neutron stars is an old subject. It can be traced back from the work of the Soviet physicist Landau [1] in early 1930s, through the pioneering work of Oppenheimer and Volkoff about massive neutron cores in fully relativistic formalism in 1939 [2]. The discovery of radio pulsars by Bell and Hewish [3] in 1967 made clear that the nuclear forces became repulsive at low distances due to the pulsar masses. Nowadays we believe that the EoS of nuclear matter is very stiff at high densities to explain the recent discovery of the hyper massive MSP J0740+6620, whose mass range lies at $2.14^{+0.10}_{-0.09} M_{\odot}$ with 68% credibility interval and $2.14^{+0.20}_{-0.18} M_{\odot}$ with 95% credibility interval [4], as well the PSR J0348+0432 whose mass lies between $2.01 \pm 0.04 M_{\odot}$ [5].

On the other hand, quantitative results about neutron stars radii only significantly evolve in the last decade. The radius of canonical $1.4M_{\odot}$ in the past was estimated around 17 km [6]. Until today even more conservative results have pointed out that the radius of canonical stars cannot surpass 14 km [7–11]. More radical studies point to a maximum radius close to 13 km [12–14], and a very recent study constrains the maximum radius to only 11.9 km [15].

We can divide the neutron star in four distinct parts: the outer crust, the inner crust, the outer core and the inner core. It is well accepted that the symmetry energy slope at the saturation density - which corresponds to the outer core region - is the main responsible for controlling the neutron stars radii. Although some studies suggest that this cannot be the whole history [16, 17], it is undeniable that the symmetry energy slope plays more than a significant role [14, 18–22].

In this work, nevertheless, I explore another region of the neutron star: the inner crust. Instead of build a model for it, I study only its behaviour, using an empirical parametrization for the EoS: $p(\epsilon) = K \cdot \epsilon^{\gamma} + b$, where we varying the value of γ and determine the value of the constants K and b in order to keep the pressure continuous. Also, in order to gain physical insight, I cal-

culated the speed of sound of the inner crust. I show that although for all γ values we always have a monotonically increasing EoS, we have very distinct behaviour for the speed of sound as well as different values of the radius of the canonical mass.

II. THE NEUTRON STAR LAYERS.

As pointed out earlier, the neutron star can be divided in four distinct regions: outer crust, inner crust, outer core and inner core.

A. Outer crust

The outer crust is the region considered in the range $10^{-14} \text{ fm}^{-3} \lesssim n \lesssim 10^{-4} \text{ fm}^{-3}$, where the ground state of nuclear matter is such that all neutrons are bound in nuclei, and that it forms a perfect crystal with a single nuclear species, (number of neutrons N , number of protons Z), at lattice sites. The formulation of this model is known today as BPS model [23]. For densities up to 10^{-9} fm^{-3} the ground state is a body-centered-cubic (bcc) crystal lattice of ^{56}Fe with negligible - but increasing - pressure. For higher densities, the matter is a plasma of nuclei and electrons which form a nearly uniform Fermi gas and the degenerescence pressure of electrons, as well as the lattice pressure - due to the Coulomb interactions - become relevant. For densities above 10^{-7} fm^{-3} the ^{56}Fe is no longer the ground state of the matter but the ^{62}Ni is. Therefore, a sequence of increasingly neutron rich nuclei follows, and ends up in the ^{78}Ni for density around 10^{-4} fm^{-3} [24].

The ground state composition at a given density corresponds to the absolute minimum of the baryon chemical potential in the N - Z plane. Typically, there is only one well distinguished minimum. A well pronounced second minimum appears only close to the transition density between two nucleus species. With increasing density it becomes a new absolute minimum. (For a complete relation between a given density and the corresponding ground state nucleus, as well as a longer discussion about the outer crust see ref. [24]). In this work I use the BPS EoS to the outer crust.

* llopes@cefetmg.br

B. Inner crust

The inner crust is the region comprehending around $10^{-4}\text{fm}^{-3} \lesssim n \lesssim 10^{-1}\text{fm}^{-3}$. Here, very neutron rich nuclei are immersed in a gas of dripped neutrons [24].

In general, calculations of the structure, composition, and equation of state of the inner crust can be divided into three groups, alongside many subgroups within different parametrizations, techniques and approximations: Full quantum mechanical treatment can be carried out within the Hartree-Fock (HF) approximation with an effective nucleon-nucleon interaction as done in ref. [25]. Further approximation of the many-body wave function can be done using semi-classical Extended Thomas-Fermi (ETF) approximation. Basic quantities within the ETF are neutron and proton densities and their spatial gradients, as done in ref. [26]. Finally, investigations belonging to the third group use Compressible Liquid Drop Model (CLDM) parametrization for the description of nuclei, with parameters derived within a microscopic nuclear many-body theory as done in ref. [27] (called BBP EoS).

Besides the uncertain discussed above, close to the inner crust edge the competition between attractive nuclear force and repulsive Coulomb interaction can turn the nuclear matter into a frustrated system, i.e, the system presents more than one low-energy configuration, which can cause the onset of unusual nuclear shapes with different geometries. This is called nuclear pasta phase [28]. As pointed out in ref. [29], the presence and extension of the pasta phase is strongly model dependent. While ref. [30] stated that there is no pasta phase, ref. [31, 32] shows that pasta phase is present for densities from 0.006fm^{-3} to 0.1fm^{-3} .

As can be seen from the discussion above, the inner crust up to date still present significant ambiguities. Therefore, instead of analyze different models alongside several parametrizations, with and without pasta phase, I construct here an empirical study of the inner crust for $0.003\text{fm}^{-3} < n < 0.08\text{fm}^{-3}$ within a polytropic EoS:

$$p(\epsilon) = K \cdot \epsilon^\gamma + b, \quad (1)$$

where p is the pressure and ϵ is the energy density.

Now, it is very important to emphasize that the pressure needs be kept continuum in the outer crust-inner crust transition, as well as in the inner crust-core tran-

sition. To accomplish this task, for a given value of γ we need to reproduce $p = 1.509 \times 10^{-5}\text{fm}^{-4}$ for $\epsilon = 1.402 \times 10^{-2}\text{fm}^{-4}$, which is predicted by the BBP EoS at $n = 0.0029\text{fm}^{-3}$ [27]; and $p = 2.409 \times 10^{-3}\text{fm}^{-4}$ for $\epsilon = 3.838 \times 10^{-1}\text{fm}^{-4}$ at $n = 0.083\text{fm}^{-3}$, which is predicted by the Quantum Hadrodynamics (QHD) model NL ρ [33] (discussed below). This assures a continuous pressure.

It is also worth to pointing out that this is not the only possible approach. For instance, ref. [7] uses two different polytropic EoS to kept the pressure continuous.

As the NL ρ model predicts a maximum neutron star mass at $n = 1.07\text{fm}^{-3}$, we see that the analyzed region is just a small fraction of the total EoS. The parameters used in this work are displayed in Tab. I

| γ | K | b |
|----------|------------------------|-------------------------|
| 1/3 | 4.930×10^{-3} | -1.173×10^{-3} |
| 2/3 | 5.094×10^{-3} | -2.811×10^{-4} |
| 7/3 | 2.238×10^{-2} | 1.403×10^{-5} |
| 4 | 1.103×10^{-1} | 1.509×10^{-5} |
| 6 | 7.490×10^{-1} | 1.509×10^{-5} |

TABLE I. Parameters of the empirical model of the inner crust in the region $0.003\text{fm}^{-3} < n < 0.08\text{fm}^{-3}$.

C. The outer and inner core

If the density is high enough (around $0.06 - 0.1\text{fm}^{-3}$) the surface and Coulomb contributions can be ignored and the matter can be approximated by an infinite and uniform plasma of interacting protons, neutrons and free electrons (and muons if the electron Fermi energy is high enough) in chemical equilibrium. This is the outer core. Therein a very special point exists: the nuclear saturation density n_0 ($0.148 - 0.170\text{fm}^{-3}$). From this point, the nuclear forces become repulsive instead of attractive. Any reliable model for the outer core needs to predict at least six well known properties of symmetric nuclear matter at the saturation point: the saturation density itself (n_0), the effective nucleon mass (M^*/M), the compressibility (K), the symmetry energy (S_0), the binding energy per baryon (B/A) and the symmetry energy slope (L) [22, 34]. Alongside these six physical quantities, ref. [35] also constrains the EoS in the range $2.0 < n/n_0 < 4.5$.

To fulfill these constraints I use an extended version of the QHD [36] whose Lagrangian reads:

$$\begin{aligned} \mathcal{L}_{QHD} = & \sum_b \bar{\psi}_b \left[\gamma^\mu (i\partial_\mu - g_{b,\omega}\omega_\mu - g_{b,\rho}\frac{1}{2}\vec{\tau} \cdot \vec{\rho}_\mu) - (m_b - g_{b,\sigma}\sigma) \right] \psi_b + \frac{1}{2}m_v^2\omega_\mu\omega^\mu \\ & + \frac{1}{2}m_\rho^2\vec{\rho}_\mu \cdot \vec{\rho}^\mu + \frac{1}{2}(\partial_\mu\sigma\partial^\mu\sigma - m_s^2\sigma^2) - U(\sigma) - \frac{1}{4}\Omega^{\mu\nu}\Omega_{\mu\nu} - \frac{1}{4}\mathbf{P}^{\mu\nu} \cdot \mathbf{P}_{\mu\nu}, \end{aligned} \quad (2)$$

in natural units. ψ_b are the nucleon Dirac fields. The σ , ω_μ and $\vec{\rho}_\mu$ are the mesonic fields. The g 's are the Yukawa coupling constants that simulate the strong interaction, m_b is the mass of the baryon b , m_s , m_v , and m_ρ are the masses of the σ , ω , and ρ mesons respectively.

The $U(\sigma)$ is the self-interaction term introduced in ref. [37] to reproduce some of the saturation properties of the nuclear matter and is given by:

$$U(\sigma) = \frac{1}{3!}\kappa\sigma^3 + \frac{1}{4!}\lambda\sigma^4. \quad (3)$$

As neutron stars are stable macroscopic objects, we need to describe a neutral, chemically stable matter and hence, leptons are added as free Fermi gases. In Tab. II, I display the parameters of the NL ρ model as well as the prediction of the physical quantities and their inferred values from phenomenology [22, 34]. Moreover, as pointed out in ref. [18, 34], the EoS constraint from ref. [35] is also fully satisfied. It also predicts a maximum mass larger than two solar mass, in agreement with ref. [4, 5].

| | Parameters | | Phenomenology | NL ρ |
|------------------------|---------------|---------------------|---------------|-----------|
| $(g_{N\sigma}/m_s)^2$ | 10.330 fm^2 | n_0 (fm^{-3}) | 0.148 - 0.170 | 0.16 |
| $(g_{N\omega}/m_v)^2$ | 5.421 fm^2 | M^*/M | 0.7 - 0.8 | 0.75 |
| $(g_{N\rho}/m_\rho)^2$ | 3.830 fm^2 | K (MeV) | 200 - 260 | 240 |
| κ/M_N | 0.01387 | S_0 (MeV) | 30 - 34 | 30.49 |
| λ | -0.0288 | B/A (MeV) | 15.7 - 16.5 | 16.0 |
| M_N | 939 MeV | L (MeV) | 36 - 86.8 | 84.9 |

TABLE II. NL ρ model parameters and predictions [33] with the physical quantities inferred from experiments [22, 34].

The region with $n > 2 n_0$ is called inner core. At such densities new and exotic degrees of freedom can be present. The most common non-nucleonic degrees of freedom studied in the literature are the hyperons [24, 38–43]. Another possibility is the onset of Δ 's resonances and boson condensation [38, 44]. Even more exotic settings consider that the inner core undergoes a hadron-quark phase transition. In this case we have a hybrid star, with a quark gluon plasma (QGP) at the inner core surrounded by baryonic matter [24, 38, 45–48]. In this work I consider only nucleonic degrees of freedom, therefore the outer and the inner core can be considered as the same layer.

Furthermore, the details of the construction of a beta-stable EoS from the QHD at mean field approximation used in this work can easily be found in the literature [24, 36, 38, 43, 48].

D. Results

I construct the total EoS for the neutron stars as follows: We use the BPS [23] EoS for the outer crust and the BBP [27] EoS for the inner crust for densities up to $0.003 fm^{-3}$. The EoS for the core is given by QHD calculations with NL ρ parametrization [33] starting at $0.08 fm^{-3}$. For this model, this corresponds exactly to half of the saturation density. The small region in the inner crust in the range $0.003 fm^{-3} < n < 0.08 fm^{-3}$ is parametrized by the eq. 1. I also compare the results without this parametrization. In this case the BBP EoS is used for densities up to $0.035 fm^{-3}$ and linked directly

to the QHD EoS. This is the standard approach [24, 38], here I called it “BPS+BBP”.

I displayed in Fig. 1 the EoS for all values of γ . As pointed out earlier, the analysed region is very small, therefore the differences between the different values of γ cannot be perceived with the traditional linear plot. The differences become clear if we use logarithm scale. As can be seen, the lower the value of γ , the stiffer the EoS for the inner crust. When we link the BBP to the QHD directly, (BPS+BBP) we see that this model is similar to $\gamma = 7/3$ up to energy density of $0.01 fm^{-4}$; afterwards it becomes closer to $\gamma = 4$.

As for all values of γ we always have a monotonically increasing EoS, we can gain additional physical insight studying the behaviour of the speed of sound of the inner crust. The square of the speed of sound is defined as:

$$v_s^2 = \left| \frac{\partial p}{\partial \epsilon} \right|. \quad (4)$$

Besides the effect of different speeds of sounds of the crust on the mass-radius relations, the speed of sound also provides us information about shear viscosity [49], tidal deformation [50] and even gravitational waves signatures [51]. At high densities the speed of sound is also relevant in the study of hadron-quark phase transition [45]. The results are showed in Fig. 2.

We see that the differences in the speed of sound are bigger than the EoS itself. For low values of γ we have a decrease of the speed of sound with the density. As for higher values, we have a quickly increasing speed of sound. In the case in which we have the BBP EoS linked to the QHD (BPS+BBP) we see the same behaviour of

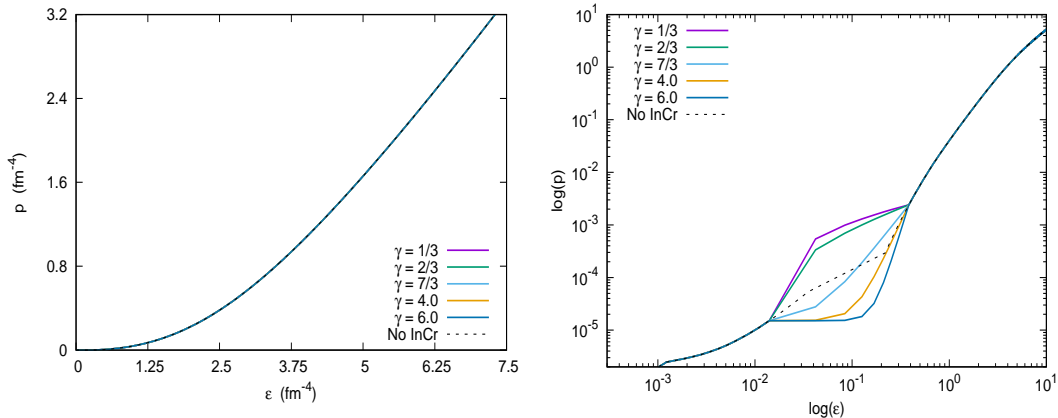


FIG. 1. (Colour online) Different EoS for the inner crust in linear (left) and logarithm (right) scales. The differences cannot be perceived in the linear scale.

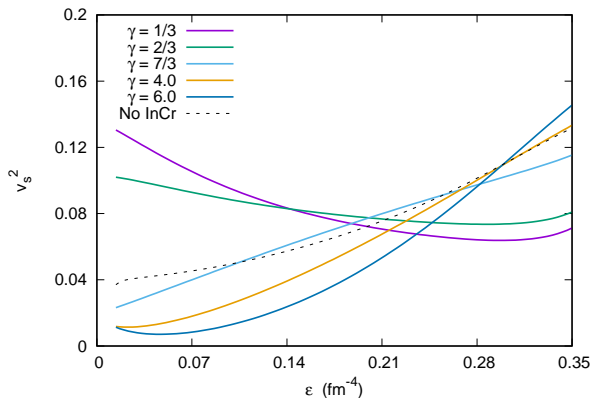


FIG. 2. (Colour online) Square of the speed of sound in the parameterized inner crust for different values of γ .

the EoS. At low energy density the speed of sound is close to $\gamma = 7/3$ and therefore closer to $\gamma = 4$.

Also, as pointed out in ref. [52], we expect a first order phase transition at the Inner Crust-core surface. Therefore, unlike the pressure, the speed of sound can present discontinuity.

Once I discussed the behaviour of the EoS and the speed of sound of the inner crust I finish the task by solving the TOV equations [2] to see how these different behaviours affects the mass-radius relation to the maximum mass and the canonical $1.4M_{\odot}$. Finally, with the mass-radius relation, I also calculate the gravitational surface redshift, defined as [7]:

$$z = \left(1 - \frac{2GM}{Rc^2}\right)^{-1/2} - 1. \quad (5)$$

The results are plotted in fig. 3 and summarized in Tab. III. As can be seen, my results point to the fact that while the inner crust does not affect the maximum mass (indeed, the central density for all maximum mass stars

is 1.07 fm^{-3}), it can play a major role in the radii, specially in the canonical $1.4M_{\odot}$. For lower values of γ , we found big radii for the canonical masses, reaching 13.87 km. For $\gamma = 6$ we found a radius of 12.75 for the 1.4 solar mass star, a difference of 1.1 km. For the "BPS+BBP" we see that the results are numerically equivalent to $\gamma = 7/3$. I also checked the inner crust effects with different parametrizations (as GM1 [53]) and found the same qualitative results.

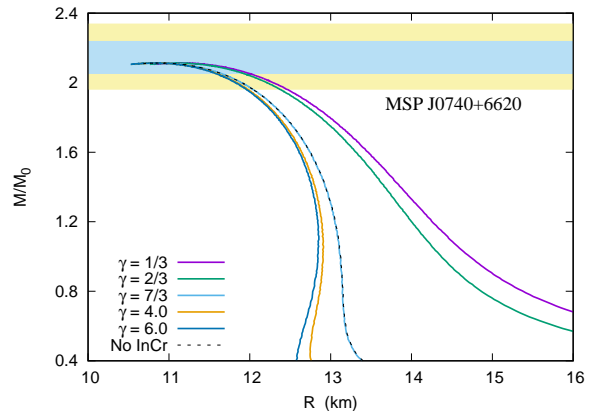


FIG. 3. (Colour online) Mass-radius relations for different values of γ . The light blue (yellow) region corresponds to the credibility interval of 68% (95%).

| γ | M/M_{\odot} | R (km) | $z_{1.4}$ | $R_{(1.4)}$ | $n_{c(1.4)}$ |
|----------|---------------|--------|-----------|-------------|--------------|
| 1/3 | 2.11 | 11.13 | 0.195 | 13.87 | 0.42 |
| 2/3 | 2.11 | 11.08 | 0.199 | 13.66 | 0.43 |
| 7/3 | 2.11 | 10.86 | 0.214 | 12.93 | 0.43 |
| 4 | 2.11 | 10.82 | 0.216 | 12.81 | 0.43 |
| 6 | 2.11 | 10.81 | 0.218 | 12.75 | 0.43 |
| BPS+BBP | 2.11 | 10.88 | 0.214 | 12.93 | 0.43 |

TABLE III. Some neutron star properties for the models discussed in the text.

On the other hand, the gravitational redshift for the canonical mass, $z_{1.4}$, varies from 0.195 to 0.218, a difference about of 10%. These values for z are in agreement of observational measures coming from the Chandra X-Ray observatory. For instance, ref. [54] points out that the redshift z of the 1E 1207.4-5209 pulsar lies between 0.12 to 0.23, although its mass and radius values are unknown.

As I fix the EoS for the neutron star core and varying only the EoS of the crust, we can compare my results with studies that make exactly the opposite: fix the EoS crust while varying the EoS of the core as done in ref. [16, 18]. Both studies vary the symmetry energy slope L while keeping all the other physical quantities unchanged and also obtain similar maximum masses. For instance, ref. [18], using non-linear ω - ρ coupling found that the radius of canonical mass can vary from 12.55 to 13.41 km, a difference of around 0.9 km (Table V of ref. [18]). On other hand ref. [16] use the additional scalar-isovector δ meson and the same NL ρ model as I use here; it found that the radius of the canonical star varying from 12.97 to 14.10, a difference of 1.1 km (Table 16 of ref. [16]). We see that the differences in the radii varying the inner crust EoS are very close to the works that vary the core EoS. This is quite impressive, as the inner crust of a canonical star is less than 20% of the total EoS.

E. Conclusions

In this work I build an empirical EoS for the inner crust and study how different behaviours affect the canonical mass neutron stars. I found that different behaviours in the speed of sound produce very different radii.

The strong constraint imposed by the GW170817, where the radius of the canonical mass cannot exceed 11.9 km [15] indicates that not only the homogeneous core EoS, but also the inhomogeneous crust EoS are needed to be known with a high degree of precision. Ref. [16, 18] indicates that a small symmetry energy slope (L) value can reduce the radius of the canonical star of about 1.1 km. On the other hand, here I show that a inner crust EoS within a quickly increasing speed of sound, also reduces the radius of the same order, an impressive result as the core EoS correspond to more than 80% of the total EoS.

It is also worth to point that ref. [55] study the effects of the inner crust using Thomas-Fermi approximation. The authors vary the parametrizations of the inner crust EoS, but fixed a single parametrization for the core EoS. They show that the variations of the inner crust can affect the radius of the canonical star up to 0.7 km. This corroborate the results pointed out in this work, that the inner crust effects are non-negligible. Nevertheless, no parameterization was able to reproduce the 11.9 km radius constraint of the GW170817 [15].

-
- [1] L. Landau, Phys. Z. Sowjetunion **1**, 285 (1932)
 - [2] J. Oppenheimer, G. Volkoff, Phys. Rev. **33**, 374 (1939).
 - [3] A. Hewish et al., Nature **217**, 709 (1968)
 - [4] H. Cromartie et al: Nat. Astr. **4**, 72 (2020)
 - [5] J. Antoniadis et al: Science **340**, 1233232 (2013)
 - [6] C. Wynn et al., Mont. Not. Roy. Astron. Soc. **375**, 821 (2007)
 - [7] K. Hebeler et al, Phys. Rev. Lett. **105**, 161102 (2010)
 - [8] T. Malik, et al., Phys. Rev. C. **98**, 035804 (2018).
 - [9] T. E. Riley et al., Astrophys. J. Lett. **887**, L21 (2019)
 - [10] M. C. Miller et al., Astrophys. J. Lett. **887**, L24 (2019)
 - [11] F. Fattoyev, J. Piekarewicz, and C. Horowitz, Phys. Rev. Lett. **120** 172702 (2018)
 - [12] B. Abbott et al, Phys. Rev. Lett. **121**, 161101 (2018)
 - [13] J.M. Lattimer and A.W. Steiner, Astrophys. J. **784**, 123 (2014)
 - [14] Lattimer & Steiner, Eur. Phys. J. A **50**, 40 (2014)
 - [15] C. Capano et al: Nat. Astr. **4**, 625 (2020)
 - [16] L. L. Lopes, D.P. Menezes, Braz. J. Phys. **44**, 744 (2014)
 - [17] L. Lopes and D. P. Menezes, J. Cosm. Astrop. Phys. **05**, 038 (2018)
 - [18] R. Cavagnoli, D. P. Menezes, C. Providencia, Phys. Rev. C **84**, 065810 (2011).
 - [19] S. Gandolfi et al., Eur. Phys. J. A **50**, 10 (2014)
 - [20] N. Alam et al., Phys. Rev. C **94** 052801(R) (2016)
 - [21] M. B. Tsang et al, Phys. Rev. C **86**, 015803 (2012)
 - [22] M. Oertel et al, Rev. Mod. Phys. **89**, 015007 (2017).
 - [23] G. Baym, C. Pethick, P. Sutherland: Astrophys. J. **170**, 299 (1971)
 - [24] P. Haensel, A.Y. Potekhin, and D.G. Yakovlev, *Neutron Stars I*, Springer, New York (2007)
 - [25] J Negele, D. Vautherin: Nucl. Phys. A **207**, 298 (1973)
 - [26] M. Brack, C. Guet, H. Hakansson: Phys. Rep. **123**, 275 (1985)
 - [27] G. Baym, H. Bethe, C. Pethick: Nucl. Phys. A **175**, 225 (1971)
 - [28] D. Ravenhall, C.. Pethick, and J. Wilson, Phys. Rev. Lett. **50**, 2066 (1983).
 - [29] C. Lorenz, D. Ravenhall, J. Pethick, Phys. Rev. Lett. **70**,379 (1993).
 - [30] F. Douchin, P. Haensel, Phys. Lett. B **485**, 107 (2000)
 - [31] S. Avancini et al., Phys. Rev. C **78**, 015802 (2008).
 - [32] S. Avancini et al., Phys. Rev. C **79**, 035804 (2009).
 - [33] B. Liu et al., Phys. Rev. C **65**, 045201 (2002)
 - [34] M. Dutra et al, Phys. Rev. C **90**, 055203 (2014).
 - [35] P. Danielewicz et al., Science **298**, 1592 (2002).
 - [36] B. D. Serot, Rep. Prog. Phys. **55**, 1855 (1992)
 - [37] J. Boguta and A.R. Bodmer, Nucl. Phys. A **292**, 413 (1977).
 - [38] N. K. Glendenning, *Compact Stars*, Springer, New York - Second Edition (2000)
 - [39] J. Ellis, J. I. Kapusta, K. A. Olive Nucl. Phys. B **348**, 345 (1991)
 - [40] R. Cavagnoli, D.P. Menezes, Braz. J. Phys. **35**, 869 (2005)
 - [41] S. Weissenborn, D. Chatterjee, and J. Schaffner-Bielich, Phys.Rev. C **85**, 065802 (2012)
 - [42] L. L. Lopes, D.P. Menezes, Phys. Rev. C **89**, 025805

- (2014)
- [43] L. L. Lopes, D.P. Menezes, Braz. J. Phys. **42**, 428 (2012)
 - [44] V. Dexheimer and S. Schramm, Astrophys. J. **683**, 943 (2008)
 - [45] E. Annala et al., Nat. Phys. **16**, 907 (2020)
 - [46] I. Sandoval, et al., Phys. Rev. C **93** , 045812 (2016).
 - [47] L. Lopes, D. Menezes Eur.Phys.J. A **56**, 122 (2020)
 - [48] L. Lopes, D. Menezes, Nucl. Phys. A **1009** , 122171 (2021)
 - [49] R. Epstein, Astrophys. J. **333**, 880 (1988)
 - [50] A. Kanakis-Pegios, P. Koliogiannis, C. Moustakidis, Phys. Rev. C **102**, 055801 (2020)
 - [51] M. Aloy et al., Mon. Not. Roy. Astron. Soc., **484**, 4980 (2019)
 - [52] L. González-Romero, J. L. Blázquez-Salcedo, AIP **1458**, 419 (2012)
 - [53] N. K. Glendenning, S. A. Moszkowski, Phys. Rev. Lett. **67**, 2414 - (1991).
 - [54] D. Sanwal et al., Astrophys. J. Lett. **574**, L61 (2002)
 - [55] I. Rather, A. Usmani, S. Patra, Nucl. Phys. A **1010** , 122189 (2021) .